Volume 13
Number 45
7 December 2022
Pages 13251–13634

Chemical Science

rsc.li/chemical-science

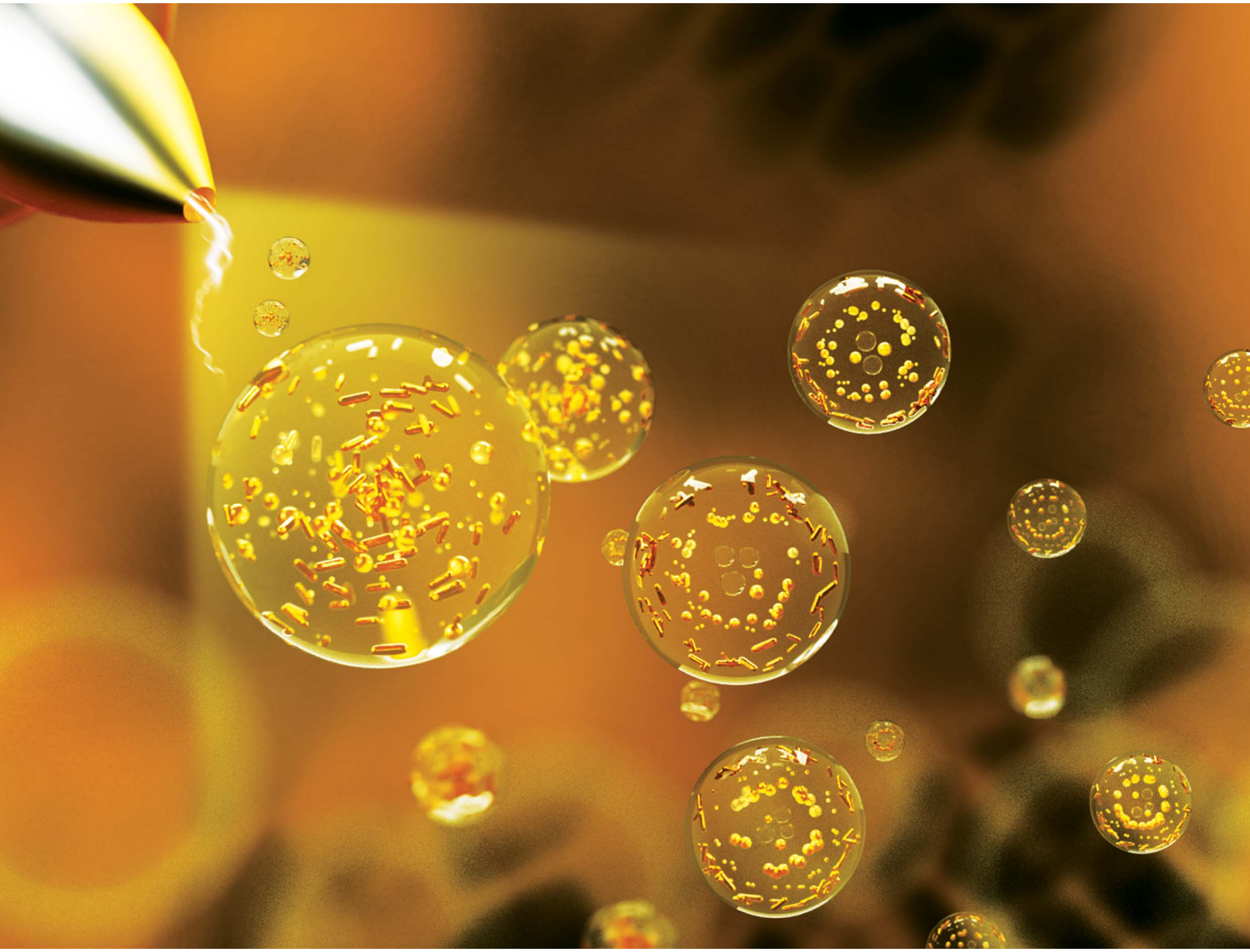

ISSN 2041-6539

ROYAL SOCIETY
OF **CHEMISTRY**

EDGE ARTICLE
Thalappil Pradeep *et al.*
Spatial reorganization of analytes in charged aqueous microdroplets

Chemical Science

ROYAL SOCIETY OF CHEMISTRY

EDGE ARTICLE

View Article Online
View Journal | View Issue

Check for updates

Cite this: *Chem. Sci.*, 2022, **13**, 13321

All publication charges for this article have been paid for by the Royal Society of Chemistry

Received 16th August 2022
Accepted 11th October 2022

DOI: 10.1039/d2sc04589c

rsc.li/chemical-science

Spatial reorganization of analytes in charged aqueous microdroplets†

Pallab Basuri,[a] Amrita Chakraborty,[a] Tripti Ahuja,[a] Biswajit Mondal,[a] Jenifer Shantha Kumar[a] and Thalappil Pradeep *[ab]

Imprinted charged aqueous droplets of micrometer dimensions containing spherical gold and silver nanoparticles, gold nanorods, proteins and simple molecules were visualized using dark-field and transmission electron microscopies. With such studies, we hoped to understand the unusual chemistry exhibited by microdroplets. These droplets with sizes in the range of 1–100 μm were formed using a home-built electrospray source with nitrogen as the nebulization gas. Several remarkable features such as mass/size-selective segregation and spatial localization of solutes in nanometer-thin regions of microdroplets were visualized, along with the formation of micro–nano vacuoles. Electrospray parameters such as distance between the spray tip and surface, voltage and nebulization gas pressure influenced particle distribution within the droplets. We relate these features to unusual phenomena such as the enhancement of rates of chemical reactions in microdroplets.

Introduction

Microdroplets formed by methods such as levitation of liquids, nebulization of bulk liquids, electrospray, microfluidics, and pressurized liquid jets, exhibit unusual behavior in comparison to their bulk counterparts.[1–7] For example, numerous organic reactions *e.g.*, Michael addition,[8] Schiff-base formation,[8,9] Claisen–Schmidt reaction,[10] Suzuki coupling,[11] benzimidazole synthesis,[12] Hantzsch reaction,[13] Biginelli reaction,[14] *etc.*, were found to occur with an acceleration factor of the order of 10^1–10^8.[15] These reactions were studied in droplets produced using electrospray sonic ionization (ESSI),[16] nanoelectrospray ionization (nESI),[17] desorption electrospray ionization (DESI),[8] or Leidenfrost effect[1] *via* on-line or off-line mass spectrometric methods. A few interfacial properties of these droplets worth noting are strong enrichment of reagent molecules,[18,19] existence of a stable pH gradient,[20] partial desolvation of the molecules,[15,21] presence of high electric field,[22] and restricted molecular rotations.[23]

Water at a heterogeneous interface shows distinct properties in terms of its molecular organization and hydrogen bond strength compared to bulk water.[24–26] Such molecular properties were mainly understood using spectroscopy at the interface. However, it is likely that performing microscopy and spectroscopy at the surface of electrosprayed microdroplets during their time of flight is tricky. As a result, most of the studies were performed using static droplets created by methods such as liquids confined in a small volume, levitated droplets, droplets in a liquid trap such as oil-in-water systems, hanging droplets, *etc.* Goy *et al.* demonstrated that rapidly evaporating aqueous microdroplets reach a supercooled condition of −42 °C.[27] Quite a few other properties of aqueous microdroplets were also realized by performing reactions using preparative electrospray ionization mass spectrometry utilizing water as a solvent. For example, aqueous microdroplets accelerate several enzymatic reactions,[28–30] induce spontaneous reduction of molecules,[31] lead to micromolar quantity of hydrogen peroxide,[32–34] favor energetically unfavorable reactions,[35,36] *etc.* Besides acceleration, they were also utilized in synthesizing nanomaterials under ambient conditions. Several nanomaterials such as gold nanoparticles,[37] metallic silver nanobrushes,[38] metallic palladium nanosheets,[39] nonstoichiometric copper sulfides,[40] *etc.*, were synthesized using ambient electrospray droplet deposition. Polydisperse metallic nanoparticles are shown to anneal to monodisperse ones in microdroplets.[41] Most of the microdroplet chemistry known today is concerning transformations of small molecules and the products were studied using in-droplet molecular spectroscopy. However, how do molecules and particles distribute within a microdroplet, is still not understood clearly.

In the past few years, microdroplets were considered as a model for membraneless protocell to understand elementary processes such as chemical transformations, replication, cell splitting, compartmentalization, *etc.*[42–45] However, this was

---

[a] *DST Unit of Nanoscience, Department of Chemistry, Indian Institute of Technology, Madras, Chennai 600036, India. E-mail: pradeep@iitm.ac.in*

[b] *International Centre for Clean Water, Chennai, Tamil Nadu 600113, India*

† Electronic supplementary information (ESI) available: DFM images of microdroplets containing silver and gold nanoparticles, TEM images of microdroplets, DFM images of dropcasted sample, characterization of AuNPs and GNRs, fluorescent images of microdroplets containing protein and dye. See DOI: **https://doi.org/10.1039/d2sc04589c**

originally proposed by Oparin over 100 years ago through which he suggested a compartmentalization model based on liquid–liquid phase separation, enrichment, and localization of electrolytes in aqueous droplets, called coacervates.[46] Interestingly, Moreau *et al.* observed that droplets formed by electrostatic complexation of poly(diallyl dimethylammonium chloride) and adenosine triphosphate (ATP) at pH 8 undergo vacuolization upon addition of a neutral molecule, tetramethylene glycol.[47] Liang *et al.* showed that poly-L-lysine (PLL) and single-stranded oligonucleotide filled microdroplets undergo circulation and vacuolization simultaneously in the presence of low electric field, such as 10^3 V m^{-1}.[48] Recently, Perez-Mercader *et al.* performed radical polymerization reactions in microdroplets and observed high structural complexity in them. Authors compared such microdroplets crowded with macromolecules with living systems to understand how molecular complexity leads to microscopic outputs.[49] Nevertheless, such dynamic behavior within droplets was not observed in electrosprayed microdroplets.

Herein, we present a method of visualizing the evolution of interfacial particle enrichment within charged aqueous microdroplets in detail through optical and electron microscopy. A home-built electrospray ion source was used to create these microdroplets containing silver and gold nanoparticles (Au and AgNPs), gold nanorods (GNRs), a fluorescent-molecule tagged protein, and a fluorescent dye, both separately as well as in the form of binary mixtures. Imprints of these droplets on different surfaces were imaged using dark-field and transmission electron microscopies (TEM). The distribution of particles within the droplets were investigated at various electrospray parameters. Exceptional features such as spatial localization, following concentration gradient by mass and size-selective sorting of particles has been observed. We also observed formation of vacuoles in electrospray microdroplets displaying unprecedented analyte distribution.

Results and discussion

Understanding aqueous microdroplets containing silver and gold nanoparticles

Colloidal aqueous Ag and Au NPs prepared by the Turkevich method (synthetic protocol is presented in Experimental section) were electrosprayed using a home-built electrospray source. During spray, a 0.145 mm thick pre-cleaned glass slide (Schott) was quickly (~1 s) exposed to the spray plume to take imprints of the generated microdroplets on the glass surface. These imprinted droplets were transferred to the sample stage of a dark-field microscope for imaging.[50] Fig. 1A schematically presents the droplet imprinting setup and Fig. 1B shows a schematic of the confocal microscopy set-up for dark field imaging. In dark-field microscopy (DFM), the sample surface was scanned to obtain a series of images. Microdroplets with varying shapes and sizes were seen.

Droplet impact-induced pattern formation on solid surfaces is known.[51,52] And this is likely in electrospray deposition as well. However, upon careful inspection of ~200 droplets per cm^2 per s, we understood that AgNPs arrange commonly in two ways. In the first, they were distributed evenly in the droplet, while in the second, there was more localization at the periphery. Fig. 1C shows a DFM image of a selected area of the glass slide where these two types of droplets are seen. Droplets marked with green squares, called NP1, had an even distribution of particles throughout. Whereas droplets marked with red squares, called NP2, show strong enrichment of AgNPs towards the periphery. In latter droplets, the core of the droplet either has no or reduced particle density. A few other images are also shown in Fig. S1† wherein several such droplets of both types were observed. We found an approximate distribution of NP1 and NP2 droplets in the ratio of 3 : 7. The observation of NP1 contradicts one of the common hypotheses and a recent observation that reagents are predominantly enriched at the air–liquid interface in electrosprayed microdroplets.[18,19] Rather, we assed that concentration gradient of reagents is highly influenced by the flight time of the droplet. This apparent difference made us explore imprint imaging further. A similar phenomenon was observed with droplets of AuNPs as well, shown in Fig. S2.†

Electrospray is known to affect particles in the droplet.[41] To understand any possible change in the particle shape and size, we performed TEM measurements. A detailed description of the sample preparation for TEM is in the Experimental section. Note that imprinting an individual droplet with perfect shape and size on a TEM grid is difficult and requires several attempts. Configuration of the TEM sample preparation set-up is schematically presented in Fig. S3A.† Fig. S3B† shows a TEM image of an individual droplet of approximately 10–15 μm in diameter. Strikingly, even after several attempts, we could not observe droplets of NP1 type in TEM (details are presented below). Rather we found that in all the droplets in TEM grids, AuNPs reorganized themselves towards the periphery which leads to a distribution similar to NP2. We also noticed that, while particles at the periphery are separated, some of them appear to be aggregated near the core. Collectively, the droplet appears as NP1. The size of these AuNP aggregates reduces from the center to the periphery of the droplet. Upon further magnification of this image, we observed no changes in the particle shape and size compared to the particles before (Fig. S3C†) and after (Fig. S3D†) spray. These particles are plasmonic with diameters over 20 nm and are stable in electrospray than the monolayer protected nanoparticles.[41] We note that the imprinted droplets on the TEM grid are 10 times smaller than the droplets in DFM experiments. This encouraged us to re-think that the phenomenon of particle enrichment may occur particularly in droplets below 10 μm.

The above results demonstrate that charged aqueous microdroplets generated from a single electrospray source acquire different size,[53] shape, and particle distribution. Such a different distribution can be a result of the anisotropic distribution of electric fields and forces acting on the nanoparticles within a droplet. A particle in a charged droplet experiences a centripetal force due to the rotations of the droplet, the electrostatic force resulting from the charge, and buoyancy of the liquid, and these influence the localization of the particle. We also note that upon droplet impact on the glass

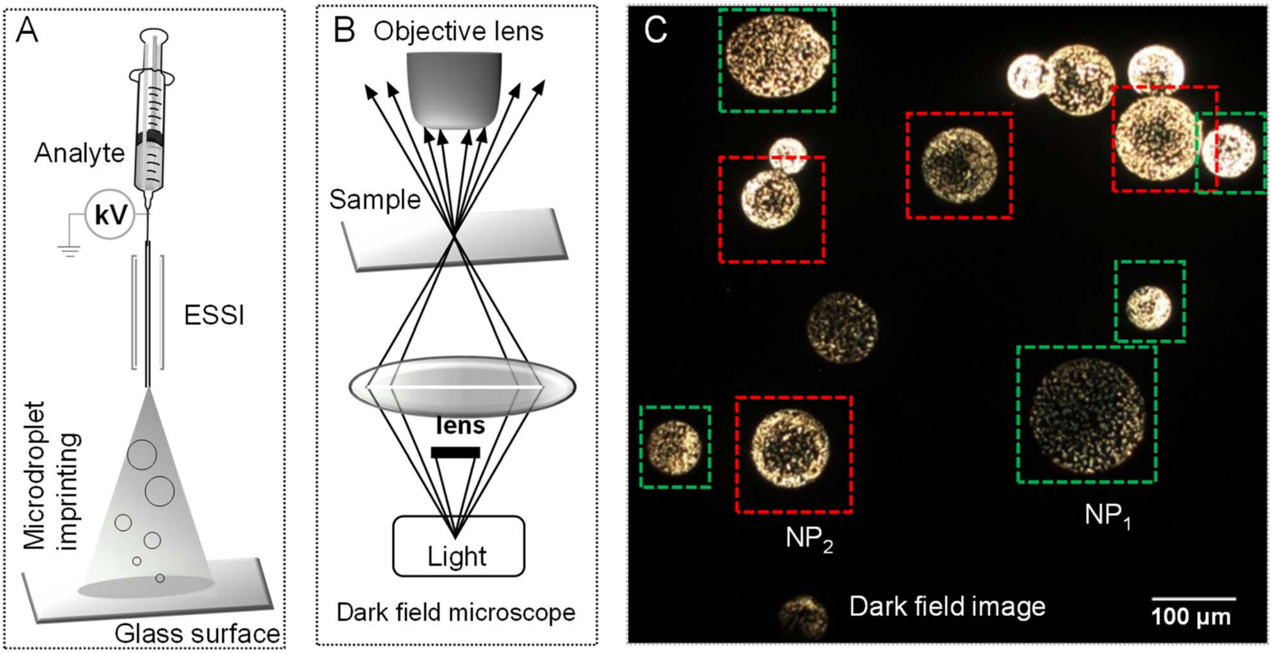

Fig. 1 Deposition and microscopy of microdroplets. (A) Schematic representation of our home-built droplet deposition setup, (B) experimental setup for dark-field microscopy of the deposited microdroplets, and (C) a representative dark-field image showing several microdroplets. Droplets are categorized into two types based on the particle size distribution; green box (NP1) and red box (NP2). Microdroplets were imprinted over a period of ∼1 s.

surface, drying may lead to an anisotropic distribution of the solute, termed as the coffee ring effect, which could have a role in the observed particle distribution.[54] The assembly of particles in an evaporating droplet was also understood theoretically.[55] A control experiment, to be discussed later, shows that droplet imprints on a glass surface, formed by simple drop casting resulted in coffee rings, but droplets imprinted by electrospray deposition, show different particle distributions. However, quantitative estimation of the forces to predict the observed particle distributions in charged microdroplets is difficult. It is noted that droplets of both types of distribution (NP1 and NP2) were seen irrespective of the size and shape of the droplet in electrospray. Besides the distribution of the nanoparticles in the droplets, DFM helps in understanding a few events of droplets occurring in their time of flight. We found a few droplets with elongated and deformed shapes. In Fig. 2A–C, we show DFM images of droplets containing AgNPs which were elongated. Such elongation of droplets in a high electric field is expected.[56] Droplet elongation and splitting are the result of a heterogeneous electric field acting across the droplet. This is one of the reasons that a droplet gets split and become small in size in flight. Apart from an elongation, a few deformed droplets

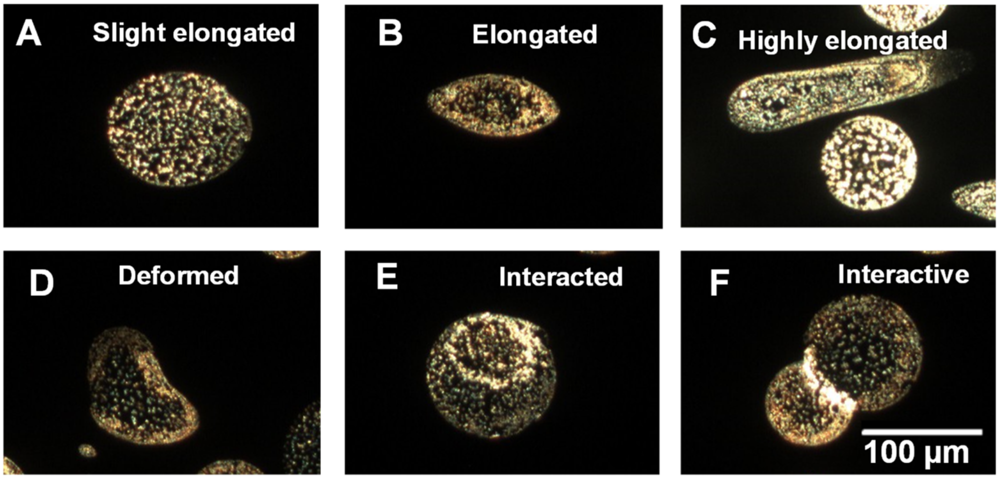

Fig. 2 Dark field images of microdroplets with different sizes and shapes demonstrating elongation (A–C), deformation (D), and interaction (E and F) of microdroplets. A few such droplets can also be found in Fig. 1 and S1† as well.

were also observed and one of them is presented in Fig. 2D. In Fig. 2E and F droplets appear to be interacting, although this may be a result of sequential deposition. Moreover, these results are consistent with the previous reports that concentration enhancement at the air–liquid interface of electrospray is indeed a part of droplet dynamics along with the change in size and shape during flight.[18]

DFM studies of droplets with mixed particles

Based on the above understanding and to gain better insights, we performed a similar experiment with GNRs to understand the effect of mass and dimensions of nanoparticles in particle distributions. GNRs were prepared in water following a seedless synthesis procedure reported by Samal *et al.*[57] The particles were characterized before the experiments using UV-vis spectroscopy and TEM. Fig. S4† shows a spectrum with characteristic peaks at 525 and 836 nm in the UV-vis spectrum, along with a TEM image of GNRs. We noticed that a few spherical gold nanoparticles were remaining in the GNR suspension. We sprayed the dispersion to take imprints of droplets on a glass surface to perform DFM analysis. A representative DFM image of a few droplets is shown in Fig. 3A where we observed droplets with different sizes and particle distributions. A few other images are presented in Fig. S5.† Upon carefully reviewing all the droplets, we categorized them into four different types, called Mix1, Mix2, Mix3, and Mix4. These 4 types are also marked with different color codes in Fig. 3A. Fig. 3B–E display representative droplets of each one of these types where the difference in particle distributions can be clearly visualized. In Mix1, marked with a green square, particles were distributed randomly without any localization or separation. In the second kind, namely Mix2, marked with a cyan square, we observed that particles tend to move towards the periphery of the droplet. These particles were further separated and localized in the third kind of droplet; Mix3, marked with a white square. Particles were finally concentrated at the periphery forming a sharp boundary which is presented as Mix4 and it is marked with a red square in Fig. 3A. By observing ~112 droplets per cm^2 per s we estimated that the percentage ratio between Mix1 : 2 : 3 : 4 follows 31 : 15 : 27 : 27. Such relocalization of particles is schematically presented in Fig. 3F. This set of data were compared with the typical coffee ring effect seen with macroscopic drops. For this, we drop cast 10 µL of as-synthesized GNR suspension on a glass surface and performed DFM after air drying. A concentration enhancement of the particles at the boundary of the drop cast sample, forming a coffee ring was observed all the time (Fig. S6†). We also observed that some particles were distributed at the interior of the drop cast sample. But these particles were distributed arbitrarily and nowhere close to the distributions of Mix1–Mix4 seen in Fig. 3.

TEM investigations of microdroplets containing mixed nanoparticles

Droplets formed by electrospray of GNR were also imprinted carefully on a copper grid, to be characterized using TEM. As

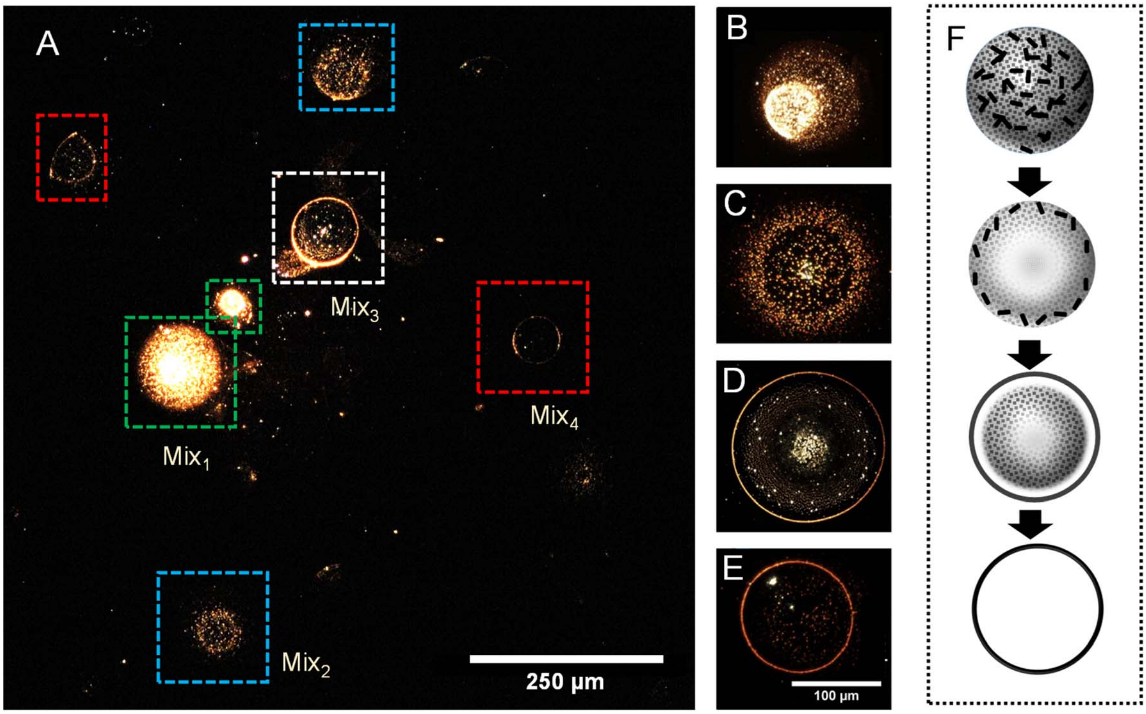

Fig. 3 Dark-field microscopy of microdroplets of aqueous solution of GNRs. These GNRs also contained a small fraction of spherical AuNPs. (A) A representative DFM image showing microdroplets of 4 different particle distributions as shown in the zoomed-in view in (B–E). Different types of droplets such as Mix1–Mix4 were marked with green, cyan, white, and red squares. (F) Mechanism of particle re-localization. The mechanism proposes particle movement (from Mix1) towards the periphery of the droplet (Mix4) *via* the formation of Mix2 and Mix3 kind of distribution, as intermediate states.

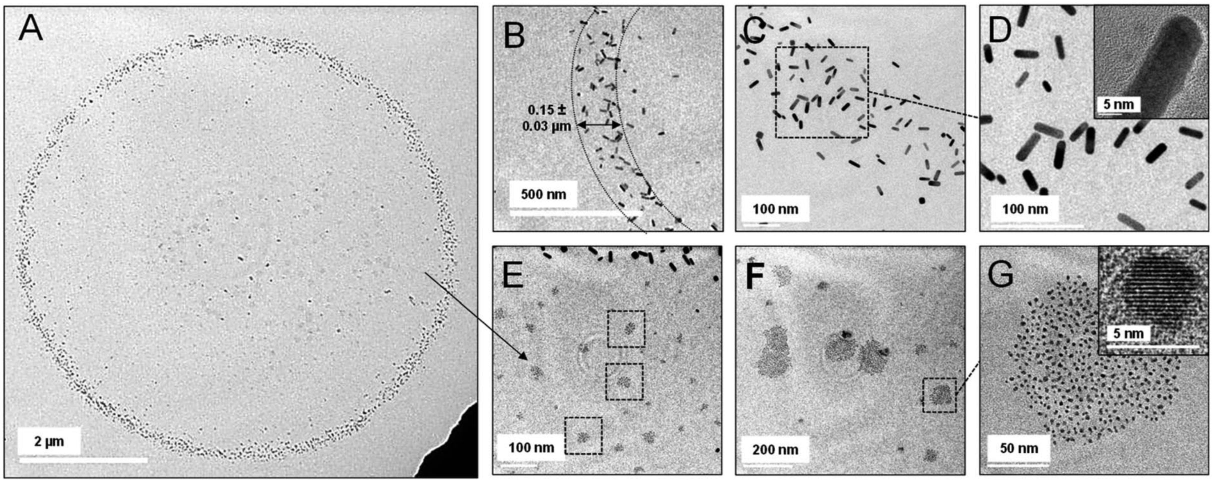

Fig. 4 TEM understanding of microdroplets formed by colloidal aqueous disperson of as-synthesized GNR. These synthesized GNR solution contain tiny fraction of AuNPs as byproducts. (A) TEM image of an individual droplet (Mix3) showing nanoparticles forming a sharp rim at the periphery. (B–D) Zoomed-in image of outer rim, showing GNRs moved to the air–water interface of the droplet. The approximate width of the rim was measured to be 0.15 ± 0.03 µm. Inset of (D) showing a single GNR at higher magnification. (E–G) The zoomed-in image showing clusters of AuNPs present at the interior of the droplet. A few of such AuNP-clusters are indicated with black squares. (G) One of such clusters of AuNPs at different magnifications. Inset of (G) showing a single AuNP at higher magnification.

expected, we could not observe Mix1 and Mix2 type of particles in the smaller droplets (below ~10 µm) imprinted on the TEM grid. However, in TEM, we found that the droplets of Mix3 show unexpected particle separation (Fig. 4). Fig. 4A displays a TEM image of a representative droplet of Mix3. Herein, we found that the droplet consists of a rim made of accumulated GNRs (Fig. 4B–D) and a few large AuNPs. Thickness of the rim is of the order of ~150 nm, as shown in Fig. 4B.

Afterward, we have taken images at higher magnifications, at the interior of the droplet. These images are presented in Fig. 4E–G wherein we can observe that the interior of the droplet is fully decorated with smaller AuNPs having no or negligible trace of GNRs. Interestingly, we found that larger aggregates of AuNP are present at the center of the droplet while smaller aggregates are found more at the periphery. Such arrangements of the AuNPs were forming concentric ring-type structures in DFM as observed in Fig. 3D. The size of these AuNPs is in the range of 5–10 nm. These AuNPs were the inseparable particles during cleaning and they were formed as a by-product in the synthesis of GNRs. Therefore, the TEM studies suggest that droplets containing mixed particles undergo chromatographic separation within the droplet and localize at the air–water interface. It should be noted that the coffee ring effect is also known to separate particles based on their size. Generally, in the coffee ring effect, smaller particles concentrate at the rim, and larger particles concentrate at the core.[54] Several attempts have been made previously to suppress the coffee ring effect either by modifying the solution or the surface.[58–60] However, in clear contrast to these previous studies, imprinted droplets in our work show four different distributions as shown above. In an electrosprayed droplet, enhanced concentrations of large nanorods were found to be at the rim whereas smaller AuNPs were distributed towards the core.

To support this further, CTAB-protected GNR and CTAC-protected AuNPs were mixed in a 1 : 1 (v/v) ratio and were sprayed. Synthesis and characterization of the as-synthesized CTAC-protected AuNPs are presented in the Experimental section and Fig. S7,† respectively. The resultant droplets were imprinted on a glass slide for DFM. As expected, we observed similar results. Herein, both the GNR and CTAC-protected AuNPs moved towards the periphery to form the outer rim and small aggregates of AuNPs rearranged at the interior. A few representative DMF and TEM images containing various types of droplets are displayed in Fig. S8A–D.† Based on the above understanding, we proposed that in-droplet particle rearrangement during time-of-flight of the droplet results in such patterned imprints on the surface. These particles finally get localized at the air–water interface making a micron-level thick rim.

Such a concentration enhancement at a thin air–liquid interface of the droplet could significantly increase both the number of collisions between reagents and the probability of reaction. Due to the increased surface area in microdroplets than in the bulk, the rate of these reactions can be accelerated. This is one of the reasons for enhanced chemical reactivity as demonstrated previously by unusual accelerated reactions.[18]

In Fig. 3F, we schematically present the mechanism of such particle localization. We assessed that particles which were initially distributed randomly get enriched at the air–water interface of the droplet over time, during flight. Therefore, the distribution of Mix2 and Mix3 are expected to be two intermediate stages of such relocalisation of particles, resulting in concentration gradient. Such a timescale is likely to depend upon the centrifugal force acting on the particle, surface tension, viscosity, and buoyancy of the liquid droplet. Effect of these physical properties in particle reorganization was observed previously in several situations such as liquid flow,[61,62] liquid/liquid interfaces,[63] cloud droplet,[64] *etc.*

Effect of electrospray parameters

To understand the effect of electrospray parameters on the properties of the droplet, aspects such as potential applied on the source, nebulization gas pressure, and tip to collector distance were varied. It is certain that the droplet size will reduce with increasing gas pressure,[65] potential,[66] distance,[67] surface tension and vapor pressure of the solvent, amount of excess charge, *etc.*[68] In Fig. S9,† we have chosen a few representative droplets from a set where we observed such an effect. Change in the distance affects the distribution of the nanoparticles within the droplet. Upon increasing the distance, the droplet size decreases and particles get time to relocate. Spatial relocalization of particles within the droplet resulted in an increase in the percentage of Mix3, as shown in Fig. S10A.† While the number density of Mix4 increases up to 2.5 cm, it falls rapidly on further increase in the distance. This could be explained by droplet desolvation resulting in no droplet imprinting at higher distances. We have seen a similar effect with decreasing gas pressure. This is because, with decreasing gas pressure, the droplet velocity also decreases with a slow rate of desolvation, which in turn allows the particle to rearrange and get localized at the air–water interface of the droplet (Fig. S10B†). The fraction of Mix1 increasing and Mix4 decreasing with nebulization pressure suggests that charge and distance are the dominant factors in particle redistribution. Fig. S10C† suggests that the applied potential follows a similar trend as the distance in particle distribution within the droplet.

Observation of vacuoles and implication to droplet reactions

While studying particle arrangements in a droplet, surprisingly, we found micron-scale bubbles inside several such droplets. Upon further magnification of DFM images, we clearly observed that bubbles of various sizes exist mostly at the core of the droplets. Fig. 5A shows a representative droplet in which several such micrometer-scale vacuoles were observed. These microvacuoles are marked with red squares. We noticed that such vacuolization has only occurred in the case of Mix3 and Mix4 and is absent in droplets of Mix1 and Mix2. This hints at the fact that the formation of such vacuoles needs some incubation time and driving force. It should also be noted that such vacuoles were not observed in the drop cast bulk dispersion (Fig. S6B†). While droplets are moving, during their time-of-flight, tiny bubbles were formed, which coalesce with each other to become big vacuoles. As a result, we observed that droplets of Mix3 contain smaller bubbles whereas, Mix4 droplets contain bigger bubbles (Fig. S11†). It should be noted that these droplets were imprinted on the same slide, in an independent experiment. It is likely that the bubbles formed in droplets are due to liquid–gas separation of the dissolved gases present in the droplet. We also noticed that particles were accumulated at the air–liquid interface of the vacuoles (Fig. 5) forming a bright rim in the DFM images. Unusual reaction rates in microdroplets have always been looked at from the perspective of enhanced concentration of the reactants at the outermost interface of the droplet; however, air–liquid interfaces of these bubbles, at the interior of the droplets have not been considered before. These additional interfaces will certainly have an important role in accelerating the chemistry in microdroplets.

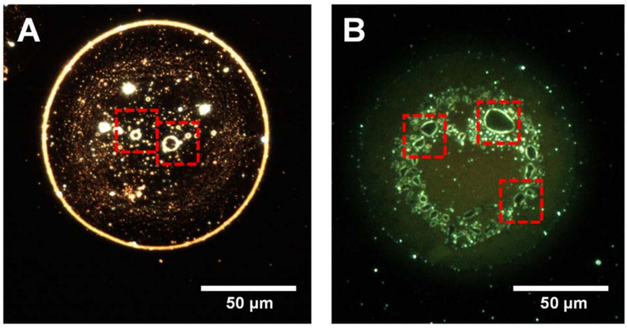

Fig. 5 Vacuolization in microdroplets. (A) DFM images of microdroplets containing as-synthesized GNR in water of Mix3. The red square showed an area with the formation of vacuoles inside of droplets. (B) DFM fluorescence image of R6G containing aqueous microdroplets with different shapes and sizes of vacuoles observed.

Particle compartmentalization and understanding of protocell formation

The nanodroplet relocalization and formation of microvacuoles motivated us to understand in-droplet particle dynamics from the perspective of the protocell model. Origin of life has been looked at from many perspectives to understand the spontaneous assembly of microscale compartments. Proteins are well known as the building blocks of cell membranes and many proteinosomes have been investigated to understand the genesis of cell membrane-bound compartments in the cells.[69] In the previous literature, the self-organization of small peptides in vesicles has been proposed as the precursor step to the formation of a protocell.[70,71] To investigate the effect of proteins in microdroplets, we have used fluorescein isothiocyanate labeled bovine serum albumin (FITC-BSA) to visualize the droplets imprinted on glass slides through DFM. Fig. S12† shows fluorescence images of several spherical and elongated droplets containing FITC-BSA. To our surprise, vacuoles were observed within the droplets, comparable to membrane-less microcompartments in biological cells.[72] One or more vacuoles were observed inside a single droplet. To neglect the effect of surfactants used for the synthesis of nanorods or large protein molecules on vacuolization, we sprayed aqueous rhodamine 6G (R6G) solution. We observed the formation of vacuoles in such droplets as well (Fig. 5B). We observed suppression of vacuolization in a degassed liquid (Fig. S13†) which further supports our hypothesis of liquid–gas phase separation within microdroplets leading to vacuole formation. Several studies are being carried out to develop a model construct of membrane-less organelles in protocells to understand the mechanism of their functions inside the cell.[73] We suggest that the formation of vacuoles in microdroplets carrying proteins and nanoparticles is comparable to such organelles. Droplets of this kind may be used to conduct further research on these processes.

Experimental

Synthesis of citrate-protected AuNPs and AgNPs in water

The colloidal aqueous suspension of citrate-caped AuNPs was synthesized using the Turkevich method, by the reduction of tetrachloroauric acid trihydrate ($HAuCl_4 \cdot 3H_2O$) using trisodium citrate.[74] An aqueous solution of 5 mM $HAuCl_4 \cdot 3H_2O$ of 10 mL was taken in a conical flask. It was then diluted with 180 mL of distilled water followed by heating until the solution started boiling. About 10 mL of 0.5% trisodium citrate was added to it and heated until the entire solution becomes wine red. In a similar way, AgNPs were made, taking $AgNO_3$ as a precursor. The dispersions were then cooled and used directly for droplet imprinting.

Synthesis of CTAB (cetyltrimethylammonium bromide)-protected GNRs in water

Gold nanorods were synthesized using a previously reported method with a few modifications.[57] Sequential addition of 2.5 mL of 10 mM $HAuCl_4 \cdot 3H_2O$, 325 μL of 10 mM $AgNO_3$, and 350 μL of 100 mM ascorbic acid to a 50 mL solution of 100 mM CTAB was performed with mild stirring at 28 °C in a synthesizer. After 5 min of incubation, a 500 μL ice-cold aqueous solution of freshly prepared $NaBH_4$ was added in one shot. The reaction mixture was kept overnight before washing the GNRs with water to get rid of the excess CTAB. The GNR dispersion was then centrifuged at 7000 rpm for 20 min to get rid of the larger particles and then centrifuged again in a stepwise fashion at 12 000 and 14 000 rpm in a similar way. The final precipitate was dispersed in deionized water and again centrifuged twice (each time for 15 min) at 12 500 rpm. The dispersion was vortexed to stop aggregation before use.

Synthesis of spherical AuNPs

A seed mediated synthetic protocol, initially reported by Xia's group, was followed to synthesize gold nanospheres.[75]

For the synthesis of initial CTAB-capped seeds, 9.75 mL 100 mM CTAB solution was thoroughly mixed with 250 μL of 10 mM $HAuCl_4$ solution in a 20 mL glass bottle. 10 mM $NaBH_4$ solution was prepared in ice cold water and 600 μL of it was quickly added to the reaction mixture. After initial stirring for 2 min, the solution was kept undisturbed for 3 h at 28 °C.

For the synthesis of CTAC (cetyltrimethylammonium chloride)-capped AuNPs, 2 mL of 200 mM CTAC solution was taken in a glass bottle. Subsequently, 1.5 mL of 100 mM ascorbic acid and 50 μL of the just prepared CTAB-capped seed solution were added to the vial under continuous stirring at 300 rpm. Finally, 2 mL of 0.5 mM $HAuCl_4$ solution was injected with one shot, and the stirring was continued for 15 min at 28 °C. The solution was then centrifuged at 14 000 rpm for 30 min, and the pellet was dispersed in DI water. The centrifugation was performed one more time and the particles were finally dispersed in 20 mM CTAC solution. To eliminate the effect of surface charge and surface ligand group on the droplet formation, we synthesized spherical AuNPs protected by CTAC, as it closely resembles CTAB that was used to prepare GNRs.

Imprinting droplets on glass slides and TEM grids

Droplets were generated using a home-built electrospray ion source. Droplets were passed through an SS-tube of 0.63 cm internal diameter and 2.5 cm of length. To do the imprinting, we exposed the imprinting surface in front of the SS-tube. This process was done as quickly as possible to avoid excessive droplet deposition on the surface. In this way, only a specific area of the surface would be exposed to the spray which will help in performing DFM. The tip to surface distance was varied. For the TEM study, a copper grid, supported on an extra clean glass slide was held in front of the SS-tube with a tweezer. The glass support was used to prevent the copper grid from bending under high gas pressure.

Dark-field optical microscopy of imprinted droplets

The dark-field imaging was done using a CytoViva™ microscope. The microscope was equipped with a high-resolution dark-field oil immersion condenser lens and a 100× oil immersion objective (UPLFLN, Olympus). An L1090-halogen lamp from International Light Technologies Inc. was used as a white light source for imaging the nanoparticles. Fluorescence imaging of microdroplets was also done on the CytoViva™ microscope with a triple bandpass filter for the green emission. A Dage Excel M cooled CCD camera was used for capturing the images. Clean glass slides (SCHOTT Nexterion®) were used for all the imaging experiments.

Conclusions

In this work, we presented in-droplet reorganization of nanoparticles and molecules contained within microdroplets, during flight. This was studied by imaging imprints of microdroplets by dark field optical microscopy and transmission electron microscopy. We propose a sequential change in the nanoparticle distribution by re-localization of particles as microdroplets move from the source to the target. In the process, nanoparticles with different sizes, morphology, and mass undergo spatial separation forming a density gradient of particle distribution. We observed an enhanced particle density at the periphery of droplets forming a sharp and ∼150 nm-thick boundary in the imprint. Such particle distribution alters the chemistry in the droplet. Additionally, we found the formation of nano–microvacuoles in microdroplets. Such vacuolization was also realized using protein-filled droplets and water droplets containing a dye molecule, enriched at the gas/liquid interface. These further suggest microdroplets to be a model system for the membraneless microcompartmentalization in protocells. Science demonstrated here has implications for the unusual reactivity of microdroplets in causing chemical and biological transformations.

Author contributions

P. B. and T. P. designed and performed the experiments. T. A., A. C., B. M., and J. S. K. helped in performing microscopy of imprinted droplets. P. B. wrote the initial draft of the paper and it was finalised with input from all the authors. The project was conceived under the supervision of T. P.

Conflicts of interest

There are no conflicts to declare.

Acknowledgements

P. B., B. M., T. A. and J. S. K. thank IIT Madras for their research fellowships. A. C. thanks CSIR for her fellowship.

References

1 R. M. Bain, C. J. Pulliam, F. Thery and R. G. Cooks, *Angew. Chem., Int. Ed.*, 2016, **55**, 10478–10482.
2 K. Aoki and K. Hasegawa, *AIP Adv.*, 2020, **10**, 55115.
3 C. Liu, J. Li, H. Chen and R. N. Zare, *Chem. Sci.*, 2019, **10**, 9367–9373.
4 M. Yamashita and J. B. Fenn, *J. Phys. Chem.*, 1984, **88**, 4451–4459.
5 A. B. Theberge, F. Courtois, Y. Schaerli, M. Fischlechner, C. Abell, F. Hollfelder and W. T. S. Huck, *Angew. Chem., Int. Ed.*, 2010, **49**, 5846–5868.
6 L. Kong, T. Lan, J. Chen, K. Wang and H. Sun, *Processes*, 2020, **8**, 676.
7 P. Ben-Tzvi and W. Rone, *Microsyst. Technol.*, 2010, **16**, 333–356.
8 M. Girod, E. Moyano, D. I. Campbell and R. G. Cooks, *Chem. Sci.*, 2011, **2**, 501–510.
9 R. M. Bain, C. J. Pulliam, S. T. Ayrton, K. Bain and R. G. Cooks, *Rapid Commun. Mass Spectrom.*, 2016, **30**, 1875–1878.
10 T. Müller, A. Badu-Tawiah and R. G. Cooks, *Angew. Chem., Int. Ed.*, 2012, **51**, 11832–11835.
11 P. W. Fedick, K. Iyer, Z. Wei, L. Avramova, G. O. Capek and R. G. Cooks, *J. Am. Soc. Mass Spectrom.*, 2019, **30**, 2144–2151.
12 P. Basuri, L. E. Gonzalez, N. M. Morato, T. Pradeep and R. G. Cooks, *Chem. Sci.*, 2020, **11**, 12686–12694.
13 R. M. Bain, C. J. Pulliam and R. G. Cooks, *Chem. Sci.*, 2015, **6**, 397–401.
14 N. Sahota, D. I. AbuSalim, M. L. Wang, C. J. Brown, Z. Zhang, T. J. El-Baba, S. P. Cook and D. E. Clemmer, *Chem. Sci.*, 2019, **10**, 4822–4827.
15 Z. Wei, Y. Li, R. G. Cooks and X. Yan, *Annu. Rev. Phys. Chem.*, 2020, **71**, 31–51.
16 S. Banerjee and R. N. Zare, *Angew. Chem., Int. Ed.*, 2015, **54**, 14795–14799.
17 R. M. Bain, S. T. Ayrton and R. G. Cooks, *J. Am. Soc. Mass Spectrom.*, 2017, **28**, 1359–1364.
18 H. Xiong, J. K. Lee, R. N. Zare and W. Min, *J. Phys. Chem. B*, 2020, **124**, 9938–9944.
19 S. Lhee, J. K. Lee, J. Kang, S. Kato, S. Kim, R. N. Zare and H. G. Nam, *Sci. Adv.*, 2020, **6**, eaba0181.
20 H. Wei, E. P. Vejerano, W. Leng, Q. Huang, M. R. Willner, L. C. Marr and P. J. Vikesland, *Proc. Natl. Acad. Sci. U. S. A.*, 2018, **115**, 7272–7277.
21 S. Mondal, S. Acharya, R. Biswas, B. Bagchi and R. N. Zare, *J. Chem. Phys.*, 2018, **148**, 244704.
22 H. Xiong, J. K. Lee, R. N. Zare and W. Min, *J. Phys. Chem. Lett.*, 2020, **11**, 7423–7428.
23 J. Kang, S. Lhee, J. K. Lee, R. N. Zare and H. G. Nam, *Sci. Rep.*, 2020, **10**, 1–10.
24 K. Tomobe, E. Yamamoto, D. Kojić, Y. Sato, M. Yasui and K. Yasuoka, *Sci. Adv.*, 2017, **3**, e1701400.
25 J. Grdadolnik, F. Merzel and F. Avbelj, *Proc. Natl. Acad. Sci. U. S. A.*, 2017, **114**, 322–327.
26 P. Ball, *Chem. Rev.*, 2008, **108**, 74–108.
27 C. Goy, M. A. C. Potenza, S. Dedera, M. Tomut, E. Guillerm, A. Kalinin, K.-O. Voss, A. Schottelius, N. Petridis, A. Prosvetov, G. Tejeda, J. M. Fernández, C. Trautmann, F. Caupin, U. Glasmacher and R. E. Grisenti, *Phys. Rev. Lett.*, 2018, **120**, 15501.
28 K. J. Vannoy, I. Lee, K. Sode and J. E. Dick, *Proc. Natl. Acad. Sci. U. S. A.*, 2021, **118**, e2025726118.
29 X. Zhong, H. Chen and R. N. Zare, *Nat. Commun.*, 2020, **11**, 1049.
30 B. J. Burris and A. K. Badu-Tawiah, *Anal. Chem.*, 2021, **93**, 13001–13007.
31 J. K. Lee, D. Samanta, H. G. Nam and R. N. Zare, *J. Am. Chem. Soc.*, 2019, **141**, 10585–10589.
32 J. K. Lee, K. L. Walker, H. S. Han, J. Kang, F. B. Prinz, R. M. Waymouth, H. G. Nam and R. N. Zare, *Proc. Natl. Acad. Sci. U. S. A.*, 2019, **116**, 19294–19298.
33 J. K. Lee, H. S. Han, S. Chaikasetsin, D. P. Marron, R. M. Waymouth, F. B. Prinz and R. N. Zare, *Proc. Natl. Acad. Sci. U. S. A.*, 2020, **117**, 30934–30941.
34 C. Zhu and J. S. Francisco, *Proc. Natl. Acad. Sci. U. S. A.*, 2019, **116**, 19222–19224.
35 I. Nam, H. G. Nam and R. N. Zare, *Proc. Natl. Acad. Sci. U. S. A.*, 2018, **115**, 36–40.
36 I. Nam, J. K. Lee, H. G. Nam and R. N. Zare, *Proc. Natl. Acad. Sci. U. S. A.*, 2017, **114**, 12396–12400.
37 J. K. Lee, D. Samanta, H. G. Nam and R. N. Zare, *Nat. Commun.*, 2018, **9**, 1562.
38 D. Sarkar, M. K. Mahitha, A. Som, A. Li, M. Wleklinski, R. G. Cooks and T. Pradeep, *Adv. Mater.*, 2016, **28**, 2223–2228.
39 D. Sarkar, R. Singh, A. Som, C. K. Manju, M. A. Ganayee, R. Adhikari and T. Pradeep, *J. Phys. Chem. C*, 2018, **122**, 17777–17783.
40 A. Jana, S. K. Jana, D. Sarkar, T. Ahuja, P. Basuri, B. Mondal, S. Bose, J. Ghosh and T. Pradeep, *J. Mater. Chem. A*, 2019, **7**, 6387–6394.
41 A. R. Chowdhuri, B. K. Spoorthi, B. Mondal, P. Bose, S. Bose and T. Pradeep, *Chem. Sci.*, 2021, **12**, 6370–6377.
42 J. Li, X. Liu, L. K. E. A. Abdelmohsen, D. S. Williams and X. Huang, *Small*, 2019, **15**, 1902893.
43 M. Li, X. Huang and S. Mann, *Small*, 2014, **10**, 3291–3298.

44 T.-Y. D. Tang, M. Antognozzi, J. A. Vicary, A. W. Perriman and S. Mann, *Soft Matter*, 2013, **9**, 7647–7656.

45 H. Sakuta, F. Fujita, T. Hamada, M. Hayashi, K. Takiguchi, K. Tsumoto and K. Yoshikawa, *ChemBioChem*, 2020, **21**, 3323–3328.

46 A. I. Oparin and A. Synge, *The origin of life on the earth*, Academic Press, New York, 3rd edn, 1957.

47 N. G. Moreau, N. Martin, P. Gobbo, T.-Y. D. Tang and S. Mann, *Chem. Commun.*, 2020, **56**, 12717–12720.

48 Y. Yin, H. Chang, H. Jing, Z. Zhang, D. Yan, S. Mann and D. Liang, *Soft Matter*, 2018, **14**, 6514–6520.

49 G. Cheng, C. Lin and J. Perez-Mercader, *Small*, 2021, **17**, 2101162.

50 J. Kimling, M. Maier, B. Okenve, V. Kotaidis, H. Ballot and A. Plech, *J. Phys. Chem. B*, 2006, **110**, 15700–15707.

51 C. W. Visser, P. E. Frommhold, S. Wildeman, R. Mettin, D. Lohse and C. Sun, *Soft Matter*, 2015, **11**, 1708–1722.

52 C. Josserand and S. T. Thoroddsen, *Annu. Rev. Fluid. Mech.*, 2016, **48**, 365–391.

53 A. Hollerbach, D. Logsdon, K. Iyer, A. Li, J. A. Schaber and R. G. Cooks, *Analyst*, 2018, **143**, 232–240.

54 T.-S. Wong, T.-H. Chen, X. Shen and C.-M. Ho, *Anal. Chem.*, 2011, **83**, 1871–1873.

55 P. Lebedev-Stepanov and K. Vlasov, *Colloids Surf., A*, 2013, **432**, 132–138.

56 S. Crotti, R. Seraglia and P. Traldi, *Eur. J. Mass Spectrom.*, 2011, **17**, 85–99.

57 A. K. Samal, T. S. Sreeprasad and T. Pradeep, *J. Nanoparticle Res.*, 2010, **12**, 1777–1786.

58 S. F. Shimobayashi, M. Tsudome and T. Kurimura, *Sci. Rep.*, 2018, **8**, 17769.

59 S. Das, A. Dey, G. Reddy and D. D. Sarma, *J. Phys. Chem. Lett.*, 2017, **8**, 4704–4709.

60 Y. Li, C. Diddens, T. Segers, H. Wijshoff, M. Versluis and D. Lohse, *Proc. Natl. Acad. Sci. U. S. A.*, 2020, **117**, 16756–16763.

61 F. Picano, G. Sardina and C. M. Casciola, *Phys. Fluids*, 2009, **21**, 93305.

62 Y. Gao, P. Magaud, L. Baldas and Y. Wang, *Micromachines*, 2021, **12**, 198.

63 J. K. Kim, P. A. Rühs, P. Fischer and J. S. Hong, *Rheol. Acta*, 2013, **52**, 327–335.

64 B. R. Bzdek, J. P. Reid, J. Malila and N. L. Prisle, *Proc. Natl. Acad. Sci. U. S. A.*, 2020, **117**, 8335–8343.

65 R. Wang, P. Allmendinger, L. Zhu, A. J. Gröhn, K. Wegner, V. Frankevich and R. Zenobi, *J. Am. Soc. Mass Spectrom.*, 2011, **22**, 1234–1241.

66 Y. Gan, Z. Jiang, H. Li, Y. Luo, X. Chen, Y. Shi, Y. Yan and Y. Yan, *Sci. Rep.*, 2019, **9**, 18791.

67 A. Wortmann, A. Kistler-Momotova, R. Zenobi, M. C. Heine, O. Wilhelm and S. E. Pratsinis, *J. Am. Soc. Mass Spectrom.*, 2007, **18**, 385–393.

68 P. Kebarle and U. H. Verkerk, *Mass Spectrom. Rev.*, 2009, **28**, 898–917.

69 X. Huang, M. Li, D. C. Green, D. S. Williams, A. J. Patil and S. Mann, *Nat. Commun.*, 2013, **4**, 2239.

70 M. Abbas, W. P. Lipiński, J. Wang and E. Spruijt, *Chem. Soc. Rev.*, 2021, **50**, 3690–3705.

71 M. Fishkis, *Orig. Life Evol. Biosph.*, 2007, **37**, 537–553.

72 S.-P. Wei, Z.-G. Qian, C.-F. Hu, F. Pan, M.-T. Chen, S. Y. Lee and X.-X. Xia, *Nat. Chem. Biol.*, 2020, **16**, 1143–1148.

73 C. Donau, F. Späth, M. Sosson, B. A. K. Kriebisch, F. Schnitter, M. Tena-Solsona, H.-S. Kang, E. Salibi, M. Sattler, H. Mutschler and J. Boekhoven, *Nat. Commun.*, 2020, **11**, 5167.

74 J. Kimling, M. Maier, B. Okenve and V. Kotaidis, *J. Phys. Chem. B*, 2006, **110**, 15700–15707.

75 Y. Zheng, X. Zhong, Z. Li and Y. Xia, *Part. Part. Syst. Charact.*, 2014, **31**, 266–273.